



ARL-TR-9322 • SEP 2021



Linear Parameter Varying (LPV) Model Predictive Control (MPC) of a High-Speed Projectile

by Joshua T Bryson and Benjamin C Gruenwald

Approved for public release: distribution unlimited.

NOTICES

Disclaimers

The findings in this report are not to be construed as an official Department of the Army position unless so designated by other authorized documents.

Citation of manufacturer's or trade names does not constitute an official endorsement or approval of the use thereof.

Destroy this report when it is no longer needed. Do not return it to the originator.



Linear Parameter Varying (LPV) Model Predictive Control (MPC) of a High-Speed Projectile

Joshua T Bryson and Benjamin C Gruenwald
*Weapons and Materials Research Directorate,
DEVCOM Army Research Laboratory*

REPORT DOCUMENTATION PAGE

*Form Approved
OMB No. 0704-0188*

Public reporting burden for this collection of information is estimated to average 1 hour per response, including the time for reviewing instructions, searching existing data sources, gathering and maintaining the data needed, and completing and reviewing the collection information. Send comments regarding this burden estimate or any other aspect of this collection of information, including suggestions for reducing the burden, to Department of Defense, Washington Headquarters Services, Directorate for Information Operations and Reports (0704-0188), 1215 Jefferson Davis Highway, Suite 1204, Arlington, VA 22202-4302. Respondents should be aware that notwithstanding any other provision of law, no person shall be subject to any penalty for failing to comply with a collection of information if it does not display a currently valid OMB control number.

PLEASE DO NOT RETURN YOUR FORM TO THE ABOVE ADDRESS.

| | | | | | |
|---|------------------------------------|---|---|--|--|
| 1. REPORT DATE (DD-MM-YYYY) September 2021 | | 2. REPORT TYPE Technical Report | | 3. DATES COVERED (From - To) 1 January–31 August 2021 | |
| 4. TITLE AND SUBTITLE Linear Parameter Varying (LPV) Model Predictive Control (MPC) of a High-Speed Projectile | | | | 5a. CONTRACT NUMBER | |
| | | | | 5b. GRANT NUMBER | |
| | | | | 5c. PROGRAM ELEMENT NUMBER | |
| 6. AUTHOR(S) Joshua T Bryson and Benjamin C Gruenwald | | | | 5d. PROJECT NUMBER | |
| | | | | 5e. TASK NUMBER | |
| | | | | 5f. WORK UNIT NUMBER | |
| 7. PERFORMING ORGANIZATION NAME(S) AND ADDRESS(ES) DEVCOM Army Research Laboratory ATTN: FCDD-RLW-WD Aberdeen Proving Ground, MD 21005 | | | | 8. PERFORMING ORGANIZATION REPORT NUMBER ARL-TR-9322 | |
| 9. SPONSORING/MONITORING AGENCY NAME(S) AND ADDRESS(ES) | | | | 10. SPONSOR/MONITOR'S ACRONYM(S) | |
| | | | | 11. SPONSOR/MONITOR'S REPORT NUMBER(S) | |
| 12. DISTRIBUTION/AVAILABILITY STATEMENT Approved for public release: distribution unlimited. | | | | | |
| 13. SUPPLEMENTARY NOTES ORCID ID: Joshua Bryson, 0000-0002-0753-6823 | | | | | |
| 14. ABSTRACT In this research, a model predictive control (MPC) strategy is implemented on a high-speed guided projectile. The nonlinear aerodynamics of the projectile in the longitudinal plane are approximated using a Linear Parameter Varying model, which is used in the controller optimization for state prediction across the control horizon. The choice of MPC cost function is presented to enforce reference tracking and flight stability, and the controller is demonstrated in simulation using the projectile nonlinear longitudinal aerodynamic model. | | | | | |
| 15. SUBJECT TERMS guided projectile flight control, Linear Parameter Varying model, model predictive control, high-speed flight, nonlinear aerodynamics | | | | | |
| 16. SECURITY CLASSIFICATION OF: | | | 17. LIMITATION OF ABSTRACT UU | 18. NUMBER OF PAGES 22 | 19a. NAME OF RESPONSIBLE PERSON Joshua T Bryson |
| a. REPORT Unclassified | b. ABSTRACT Unclassified | c. THIS PAGE Unclassified | | | 19b. TELEPHONE NUMBER (Include area code) (410) 306-0783 |

Contents

| | |
|---|-----------|
| List of Figures | iv |
| List of Tables | iv |
| 1. Introduction | 1 |
| 2. Airframe Description | 1 |
| 3. Linearized Dynamic Model | 3 |
| 4. Linear Parameter Varying Model | 5 |
| 5. MPC Methodology | 8 |
| 6. MPC Implementation and Results | 8 |
| 7. Conclusion | 11 |
| 8. References | 12 |
| Nomenclature | 14 |
| List of Symbols, Abbreviations, and Acronyms | 15 |
| Distribution List | 16 |

List of Figures

| | | |
|--------|---|----|
| Fig. 1 | LTV flight body in the configuration with rounded nose and 80-mm control surfaces hinged at the leading edge. Dimensions given in millimeters. | 2 |
| Fig. 2 | Numbering scheme of the movable aerodynamic surfaces, along with the deflection sign convention. View is from projectile base. | 3 |
| Fig. 3 | Surface plots of the linear model fits across α , M for each variable element in A. Black dots show the linearized model values at each point in the discretized flight envelope. | 7 |
| Fig. 4 | Simulation results showing controller performance for \tilde{A}_z reference tracking for a simulated flight across the desired M, α flight envelope | 11 |

List of Tables

| | | |
|----------|---|----|
| Table 1 | Mass properties for LTV | 2 |
| Table 2 | Longitudinal derivative terms | 4 |
| Table 3. | Equations for LPV model fit functions | 6 |
| Table 4 | Fit coefficients for LPV model | 7 |
| Table 5 | Weighting factors | 10 |

1. Introduction

Improving the maneuverability of guided projectiles enables range extension using gliding maneuvers, and terminal-phase maneuverability enables the projectile to engage imperfectly located targets and evade active protection systems.¹⁻³ Additionally, higher velocity is advantageous for many military projectile applications, particularly in the terminal phase of flight, but across the entire trajectory as well. Projectiles lacking an in-flight propulsion system rely on low-drag designs to maintain as much of the launch energy as possible.

Current research into low-drag, high-lift airframes for both supersonic and subsonic flight regimes is improving the understanding of desirable features of the airframe design while reducing design-cycle iteration time to rapidly evolve capabilities.⁴ One approach to long-range projectile design leverages a symmetric flight body with low-aspect-ratio fins for stability, lift, and control. For these designs, the static forces and moments can vary substantially with aerodynamic roll angle at moderate to high angles of attack (AoAs) desired for most maneuvers.⁵⁻⁶ These nonlinearities present a challenge to effective traditional flight-control design based on linearized plant models.

Model Predictive Control (MPC) is a popular control technique based on an online optimization approach, which is inherently well suited for constrained state and input problems.⁷ MPC was originally developed for linear plant models,⁸ and previous research has used linear projectile models to apply MPC to guided projectiles.⁹

However, for projectiles with nonlinear dynamics or expanded flight envelopes, a different approach required to adequately describe the dynamics for MPC. Several popular adaptations of MPC have been developed to control nonlinear processes over larger operational ranges.^{8,10,11} This research develops a Linear Parameter Varying (LPV) model to approximate the nonlinear dynamic behavior in the system model, and applies MPC techniques to develop a flight control system for disturbance rejection and reference tracking to control the longitudinal dynamics of an example high-speed guided projectile.

2. Airframe Description

The Laboratory Technology Vehicle (LTV) is an engineering test-bed projectile used by the US Army Combat Capabilities Development Command Army Research Laboratory to experiment with various gun-launched, guided flight and maneuver technologies. The LTV flight body was shaped through a series of

optimization analyses that identified design candidates with low drag and high lift-to-drag ratios while maintaining marginal stability across the supersonic Mach regime.⁴⁻⁶ The body is 105 mm in diameter and 10 cal. (1.05 m) in length with a 0.5-cal. 7° boattail, and has a center of gravity (CG) located 56% back from the nose. The projectile has a 30% ogive nose as a trade-off between drag and payload volume. There are four low-aspect-ratio fins arrayed symmetrically around the body. The projectile is designed to be sabot-launched from an 8-inch-diameter gun with no deploying aerodynamic surfaces, which limits the fin span to 8 inches tip to tip. Figure 1 shows an illustration of the LTV flight body in a configuration with a 10.5-mm-radius rounded nose tip and 80-mm chord control surfaces hinged at their leading edges. The mass properties for this variant are given in Table 1.

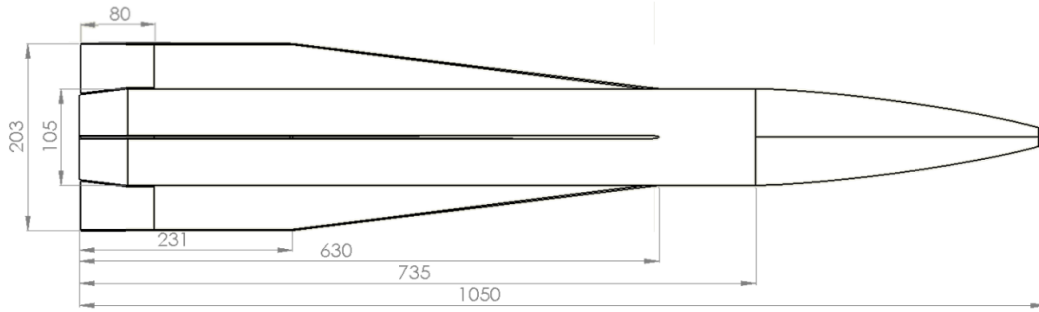


Fig. 1 LTV flight body in the configuration with rounded nose and 80-mm control surfaces hinged at the leading edge. Dimensions given in millimeters.

Table 1 Mass properties for LTV

| | |
|-----------------------------------|--------------------------|
| Mass | 16.8 kg |
| CG _X | 588 mm (56%) from nose |
| CG _Y , CG _Z | on center line |
| I_{XX} | 0.0273 kg-m ² |
| I_{YY}, I_{ZZ} | 1.247 kg-m ² |

For this analysis, the projectile is configured to fly in the “X” configuration with the roll angle location of movable surface i given by $\phi_{MAS}^i = [45^\circ, 135^\circ, 225^\circ, 315^\circ]$ for $\delta_1, \delta_2, \delta_3, \delta_4$, respectively, as illustrated in Fig. 2.

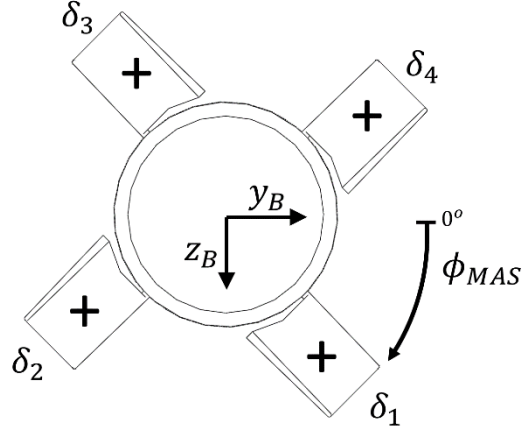


Fig. 2 Numbering scheme of the movable aerodynamic surfaces, along with the deflection sign convention. View is from projectile base.

The control mixing of the four movable surfaces into virtual control channels is given in Eqs. 1–3:

$$\delta_p = \frac{1}{4}(-\delta_1 - \delta_2 - \delta_3 - \delta_4) \quad (1)$$

$$\delta_q = \frac{1}{4}(-\delta_1 + \delta_2 + \delta_3 - \delta_4) \quad (2)$$

$$\delta_r = \frac{1}{4}(-\delta_1 - \delta_2 + \delta_3 + \delta_4) \quad (3)$$

3. Linearized Dynamic Model

For this report, the longitudinal dynamics of the projectile are considered for simplicity, but the methodology is easily extended to the full 6 degrees of freedom (6DoF) system dynamics. The expressions for the linearized longitudinal aerodynamic model and pitch-plane equations of motion for the projectile are approximated using a state space model as shown in Eqs. 4 and 5:

$$\dot{x}_p = A_p x_p + B_p \delta_q \quad (4)$$

$$y_p = C_p x_p \quad (5)$$

with the control input defined in this example as the pitch deflection, δ_q , and state vector defined as $x_p = [\theta, u, w, q]^T$, where θ is the pitch angle, u, w are the x,z velocity components, respectively, and q is the pitch angular rate. The output matrix, C_p , is the identity matrix, and the state transition matrix, A_p , and the control input matrix, B_p , are of the following form^{12,13}:

$$A_p = \begin{bmatrix} 0 & 0 & 0 & 1 \\ -g & X_u & X_w & -w_0 \\ 0 & Z_u & Z_w & u_0 \\ 0 & M_u + M_{\dot{w}}Z_u & M_w + M_{\dot{w}}Z_w & M_q + M_{\dot{w}}u_0 \end{bmatrix}, \quad B_p = \begin{bmatrix} 0 \\ X_\delta \\ Z_\delta \\ M_\delta + M_{\dot{w}}u_0 \end{bmatrix} \quad (6)$$

where u_0, w_0 , are the x,z velocity components at the linearization point (trim condition), g is the gravity term, and the partial derivative terms are calculated from the aerodynamics and mass properties at the desired trim condition as shown in Table 2.

Table 2 Longitudinal derivative terms

| | |
|--|---|
| $X_u = -\frac{QS}{mu_0}(C_{D_u} + 2C_{D_o})$ | $M_u = \frac{QSD}{u_0 I_y} C_{m_u}$ |
| $X_w = -\frac{QS}{mu_0}(C_{D_\alpha} - C_{L_o})$ | $M_w = \frac{QSD}{u_0 I_y} C_{m_\alpha}$ |
| $X_\delta = -\frac{QS}{m} C_{D_{\delta q}}$ | $M_{\dot{w}} = \frac{QSD}{u_0 I_y} \frac{D}{2u_0} C_{m_{\dot{\alpha}}}$ |
| $Z_u = -\frac{QS}{mu_0}(C_{L_u} + 2C_{L_o})$ | $M_q = \frac{QSD}{I_y} \frac{D}{2u_0} C_{m_q}$ |
| $Z_w = -\frac{QS}{mu_0}(C_{L_\alpha} + C_{D_o})$ | $M_\delta = \frac{QSD}{I_y} C_{m_{\delta q}}$ |
| $Z_\delta = -\frac{QS}{m} C_{L_{\delta q}}$ | |

In Table 2, m is the projectile mass, Q is the dynamic pressure, D is the aerodynamic reference diameter, and S is the reference area.

For this research, the plant model from Eqs. 4 and 5 is augmented with an actuator dynamic model to account for the relevant dynamics between the commanded control deflection and movement of the control surface. The actuator system is modeled as a first-order dynamic system relating the deflection command, δ_q^{CMD} , to the control surface deflection, δ_q , governed by a time constant, τ , chosen to be 0.05 s.

$$\dot{\delta}_q = -\frac{1}{\tau} \delta_q + \frac{1}{\tau} \delta_q^{CMD} \quad (7)$$

The augmented state space model combining both the projectile and actuator dynamics is given by Eqs. 8–10, with the augmented state vector defined as $x = [\theta, u, w, q, \delta_q]^T$,

$$\dot{x} = Ax + B\delta_q^{CMD} \quad (8)$$

$$y = Cx \quad (9)$$

$$A = \begin{bmatrix} A_p & B_p \\ 0 & -1/\tau \end{bmatrix}, \quad B = \begin{bmatrix} 0 \\ 1/\tau \end{bmatrix}, \quad C = \begin{bmatrix} C_p & 0 \\ 0 & 1 \end{bmatrix} \quad (10)$$

The specific aerodynamic force of the projectile in the body frame is the quantity measured by onboard accelerometers within an inertial measurement unit. The expression for the specific force component in the Z direction, \tilde{A}_Z , can be obtained as shown in Eq. 11.¹⁴

$$\begin{bmatrix} \tilde{A}_X \\ \tilde{A}_Y \\ \tilde{A}_Z \end{bmatrix} = \vec{T}_{BE}^T \left(\frac{d\vec{V}^E}{dt} - \begin{bmatrix} 0 \\ 0 \\ g \end{bmatrix} \right) = \left(\frac{d\vec{V}^B}{dt} + \vec{\omega}^B \times \vec{V}^B - \vec{T}_{BE}^T \begin{bmatrix} 0 \\ 0 \\ g \end{bmatrix} \right) \quad (11)$$

where \vec{T}_{BE}^T is the transpose of the rotation matrix from body to earth coordinates, obtained by using the standard aerospace (Z-Y-X) rotation sequence. Focusing on the Z equation, we can see that \tilde{A}_Z can be expressed as a combination of states, as shown in Eq. 12. Sign convention for this work is positive \tilde{A}_Z aligned to the $-Z$ body axis direction.

$$\tilde{A}_Z = -\dot{w} + qu + g\cos(\theta) \quad (12)$$

After substituting \dot{w} for the appropriate expression from the dynamic model in Eqs. 8–10, an expression for \tilde{A}_Z is obtained based only on the system states.

$$\tilde{A}_Z = g \cos(\theta) - Z_u u - Z_w w - Z_\delta \delta_q \quad (13)$$

4. LPV Model

The aerodynamics of the LTV are highly nonlinear with AoA, α , and the linearized model presented in the previous section is only accurate within a small region of the flight envelope surrounding the chosen linearization point.⁵ To build a controller with desired performance across a wide flight envelope, an LPV model is used to capture the majority of the nonlinear behaviors without the complexity of the full nonlinear dynamic model.¹⁵

In this LPV approach, the flight envelope is discretized by a representative sampling of linearization points, and an A , matrix is calculated at each point, according to Eqs. 6 and 9. The elements of this matrix are used to fit a polynomial function of the flight envelope parameters to approximate the full nonlinear plant dynamics across the flight envelope. This process is similar to traditional flight-controller gain scheduling, where separate linear controllers are developed for the linear model at each scheduling point; however, instead of interpolating between local controllers, the LPV interpolates between local linear models at each scheduling point. The advantage of the LPV approach is that it enables a single

controller to be designed for the entire flight envelope without requiring the use of the full nonlinear dynamic model in the onboard calculations.

For this work, the flight envelope, Γ , is defined to be at sea level, standard atmosphere with varying α , and Mach as shown in Eq. 14.

$$\Gamma : \begin{cases} 2 \leq M \leq 3.5 \\ |\alpha| \leq 12^\circ \end{cases} \quad (14)$$

The flight envelope is discretized into a set of linearization points, and the projectile is trimmed and linearized at each point $\lambda = [M, \alpha] \in \Gamma$, yielding a set of linear models of the form

$$\dot{x} = A(\lambda)x + B\delta_q^{CMD} \quad (15)$$

$$y = Cx \quad (16)$$

$$A(\lambda) = \begin{bmatrix} 0 & 0 & 0 & 1 & 0 \\ -g & A_{22}(\lambda) & A_{23}(\lambda) & A_{24}(\lambda) & A_{25}(\lambda) \\ 0 & A_{32}(\lambda) & A_{33}(\lambda) & A_{34}(\lambda) & A_{35}(\lambda) \\ 0 & A_{42}(\lambda) & A_{43}(\lambda) & A_{44}(\lambda) & A_{45}(\lambda) \\ 0 & 0 & 0 & 0 & -1/\tau \end{bmatrix} \quad (17)$$

A surface function is fitted to each variable element within $A(\lambda)$ along the flight envelope parameters α, M . The form of the fit functions for each element is chosen to include minimally sufficient complexity to adequately describe the system dynamics. Table 3 gives the formulation of the fit functions for the LPV model, and Table 4 presents the coefficients associated with each element along with the coefficient of determination for each fit, R^2 .

Table 3. Equations for LPV model fit functions

$$f_1(M, \alpha) = a + bM + c\alpha$$

$$f_2(M, \alpha) = a + bM + c\alpha + dM\alpha + e\alpha^2$$

$$f_3(M, \alpha) = a + bM + c\alpha + dM\alpha + e\alpha^2 + fM\alpha^2 + g\alpha^4$$

$$f_4(M, \alpha) = (\alpha/|\alpha|) * (a + bM + c|\alpha|) + d\sin(e|\alpha| + f)$$

$$f_5(M, \alpha) = a + bM + c|\alpha| + d\alpha^2 + e|\alpha|^3$$

Table 4 Fit coefficients for LPV model

| $A(\lambda)$ term | Fit function | R^2 | a | b | c | d | e | f | g |
|----------------------|-----------------|--------|-----------|-----------|-----------|-----------|-----------|-----------|-----------|
| A_{22} | f_2 | 0.9063 | -0.078283 | -0.003616 | 0 | 0 | -0.000447 | ... | ... |
| A_{23} | f_2 | 0.9992 | 0 | 0 | 0.003946 | -0.003169 | 0 | ... | ... |
| A_{24} | f_1 | 0.9718 | 0 | 0 | -15.964 | ... | ... | ... | ... |
| A_{25} | f_2 | 0.9225 | 0 | 0 | 0.31849 | -0.25938 | 0 | ... | ... |
| A_{32} | f_1 | 0.9840 | 0 | 0 | -0.025392 | ... | ... | ... | ... |
| A_{33} | f_3 | 0.9176 | 0.014436 | -0.86461 | 0 | 0 | -0.026971 | -0.000418 | 0.000132 |
| A_{34} | f_1 | 0.9984 | 0 | 338.31 | 0 | ... | ... | ... | ... |
| A_{35} | f_3 | 0.9590 | -0.70542 | 2.4468 | 0 | 0 | 0.04944 | -0.021008 | -2.99E-05 |
| A_{42} | f_4 | 0.9636 | 0.099861 | -0.011662 | 0.004026 | -0.085281 | 0.45937 | 1.1102 | ... |
| A_{43} | f_5 | 0.9828 | 1.658 | -0.20751 | -1.2845 | 0.14581 | -0.004767 | ... | ... |
| A_{44} | f_1 | 0.9998 | -0.21552 | -1.3393 | 0 | ... | ... | ... | ... |
| A_{45} | f_3 | 0.9576 | -4.0724 | 12.342 | 0 | 0 | 0.25517 | -0.10576 | -0.00018 |

Figure 3 plots the linear model values for the variable elements of $A(\lambda)$ at each point within the flight envelope, along with identified surface fit for each element. All fits have an R^2 value above 0.9, indicating the fit function for each element captures the majority of the variation within the data.

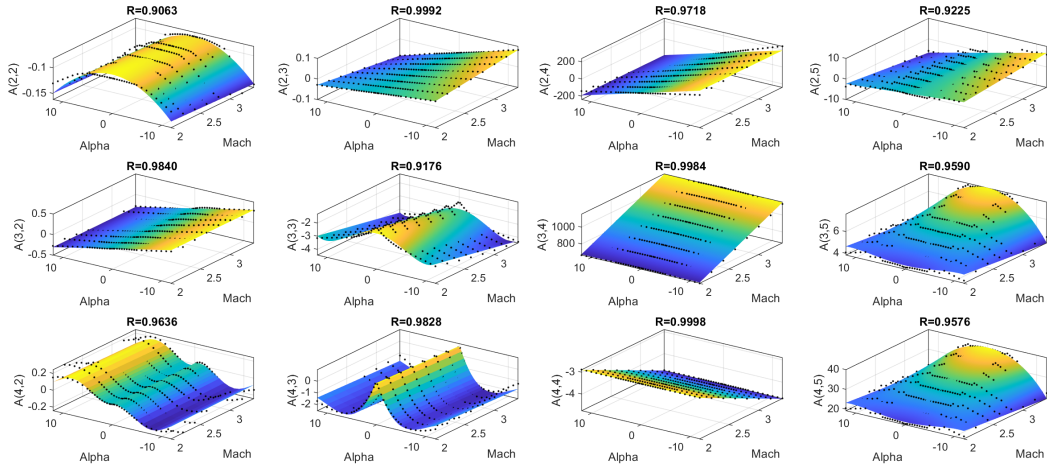


Fig. 3 Surface plots of the linear model fits across α , M for each variable element in A . Black dots show the linearized model values at each point in the discretized flight envelope.

The expression for \tilde{A}_Z from Eq. 13 can be rewritten using Eqs. 6 and 17 to be a combination of these identified fit functions, giving an approximation for \tilde{A}_Z across Γ :

$$\tilde{A}_Z = g + [0 \quad -A_{32}(\lambda) \quad -A_{33}(\lambda) \quad 0 \quad -A_{35}(\lambda)]x \quad (18)$$

5. MPC Methodology

The MPC approach uses a model of the system dynamics to forecast future system behavior and calculate the control input required to optimize the future behavior using a given cost function. The heavy reliance on the system model makes MPC a good candidate for aerospace applications that have high-quality aerodynamic characterizations and well-understood dynamics.

The general formulation of the MPC optimal control problem for a dynamic system described by $x(k+i) = f(x(k), u_c(k))$ is expressed as an optimization of the control input $u_c(k+i)$ at each time step, i , in the sliding prediction horizon of the controller, N_p . The control inputs at each time step across N_p are concatenated into a control vector, U , as shown in Eq. 19.

$$U = [u_c(k), u_c(k+1), \dots, u_c(k+N_p-1)] \quad (19)$$

The optimization seeks to identify U , which minimizes a cost function, J , across N_p , given the current state $x(k)$ while respecting a given set of constraints as shown in Eqs. 20–23.

$$\min_U J(x(k), U) = \sum_{i=0}^{N_p-1} J_i(x(k+i|k), u_c(k+i|k)) \quad (20)$$

$$s. t. \quad x(k+i) = f(x(k), u_c(k)) \quad (21)$$

$$x(k+i) \in \mathcal{X}, \forall i \in [0, N_p] \quad (22)$$

$$u_c(k+i) \in \mathcal{U}, \forall i \in [0, N_p-1] \quad (23)$$

The system dynamics across N_p are enforced by Eq. 21, while the state and control across N_p are constrained by Eqs. 22 and 23, respectively.

6. MPC Implementation and Results

MPC is often implemented using a discrete time dynamic model. However, in this work, the projectile dynamic model is used in its continuous time formulation to preserve the more conventional form of the dynamic equations and terms. The discrete time implementation can have advantages in computation time, and future research on this topic will explore moving to discrete time for hardware implementation.

The MPC is implemented using the LPV dynamics model from Eq. 15–18 along with Tables 3 and 4. The controller step time, T_s , is chosen to be 0.01 s with an N_p

of 30 steps. At each controller update, estimates of the system states are assumed to be available to the controller, $x(k)$, along with estimates of the current values of the LPV scheduling parameters, $\lambda_k = [M_k, \alpha_k]$.

Starting with these current conditions, the system states are integrated forward at each $i \in [0, N_p]$ using Runge–Kutta 4 method on the LPV model from Eqs. 15–18. The M scheduling parameter is assumed constant over N_p ($M_{k+i} = M_k$), but the α parameter is updated at each i using the w and u predicted velocities and an approximation of the arctangent function¹⁶:

$$\alpha_{k+i+1} = \frac{180}{\pi} * \frac{\left(\frac{w(k+i|k)}{u(k+i|k)}\right)}{1 + 0.28086 * \left(\frac{w(k+i|k)}{u(k+i|k)}\right)^2} \quad (24)$$

The forecasted state vectors across N_p are concatenated into a state prediction vector, X as shown in Eq. 25.

$$X = [x(k), x(k+1), \dots, x(k+N_p)] \quad (25)$$

For this implementation, no constraints are placed on the states aside from the system dynamics, but constraints to limit motion and avoid sensor saturation could be included here in future work. The control deflection is limited by a max and min deflection angle, $\delta_q^{max} = 20^\circ$, as shown in Eq. 26.

$$\mathcal{U} := \{-\delta_q^{max} \leq \delta_{q(k)} \leq \delta_q^{max}\} \quad (26)$$

The cost function for the optimization problem at each prediction step, J_i , is defined as a combination of individual costs based on the integral and proportional \tilde{A}_z tracking error, termed J_{pA_z} and J_{iA_z} , respectively, as well as costs for \dot{q} and \dot{u} , termed $J_{\dot{q}}$ and $J_{\dot{u}}$, respectively.

$$J_i = J_{\dot{q}} + J_{pA_z} + J_{iA_z} + J_{\dot{u}} \quad (27)$$

The \tilde{A}_z value is calculated across N_p using the forecasted x at each time step, and the J_{pA_z} and J_{iA_z} terms are used to enforce tracking of an \tilde{A}_z reference command, \tilde{A}_z^{REF} , through the adjustment of the Q_{pA_z} and Q_{iA_z} weighting terms, as shown in Eqs. 28 and 29.

$$J_{pA_z}(x(k+i|k), u(k+i|k)) = Q_{pA_z} * \left| \tilde{A}_z(x(k+i|k), u(k+i|k)) - A_z^{Ref} \right|^2 \quad (28)$$

$$J_{iA_z}(x(k+i|k), u(k+i|k)) = Q_{iA_z} * \left| \sum_{j=0}^i T_s * (\tilde{A}_z(x(k+j|k), u(k+j|k)) - A_z^{Ref}) \right|^2 \quad (29)$$

The $J_{\dot{q}}$ term is included in the cost function to penalize the angular acceleration and provide a stabilizing influence on the projectile through the adjustment of the $Q_{\dot{q}}$ weight factor. The controller forecasts q and the other states at each time step in N_p , and \dot{q} is approximated across N_p as shown in Eq. 30.

$$J_{\dot{q}}(x(k+i|k), u(k+i|k)) = Q_{\dot{q}} * \left| \frac{q(k+i+1|k) - q(k+i|k)}{T_s} \right|^2 \quad (30)$$

The $J_{\dot{u}}$ term penalizes changes to δ_q through the $Q_{\dot{u}}$ weighting term. This term is used to adjust the aggressiveness of the controller demands on the actuator. The controller forecasts δ_q along with the other states at each time step in N_p , and $\dot{\delta}_q$ is approximated across N_p as shown in Eq. 31.

$$J_{\dot{u}}(x(k+i|k), u(k+i|k)) = Q_{\dot{u}} * \left| \frac{\delta_q(k+i+1|k) - \delta_q(k+i|k)}{T_s} \right|^2 \quad (31)$$

The four weighting factors, Q_{pA_z} , Q_{iA_z} , $Q_{\dot{q}}$, and $Q_{\dot{u}}$ are chosen in an iterative process to control the relative prioritization of each element within the optimization. Table 5 gives the values for the weighting factor chosen for this implementation.

Table 5 Weighting factors

| | |
|---------------|--------|
| Q_{pA_z} | 0.01 |
| Q_{iA_z} | 1.0 |
| $Q_{\dot{q}}$ | 0.05 |
| $Q_{\dot{u}}$ | 0.0005 |

The MPC optimal control problem from Eqs. 20–23 is implemented in Simulink using CasADi¹⁷ and the IPOPT solver¹⁸ in a simulation using the nonlinear longitudinal aerodynamics to simulate the projectile flight. Figure 4 plots the results for an example simulation that demonstrates the ability of the MPC to control the projectile across the flight envelope. The simulation is initialized with a q of 0.5 rad/s and α of 5° at Mach 3.5. A series of alternating positive and negative A_z^{Ref} commands are closely followed by the controller as the projectile speed decreases over the simulation.

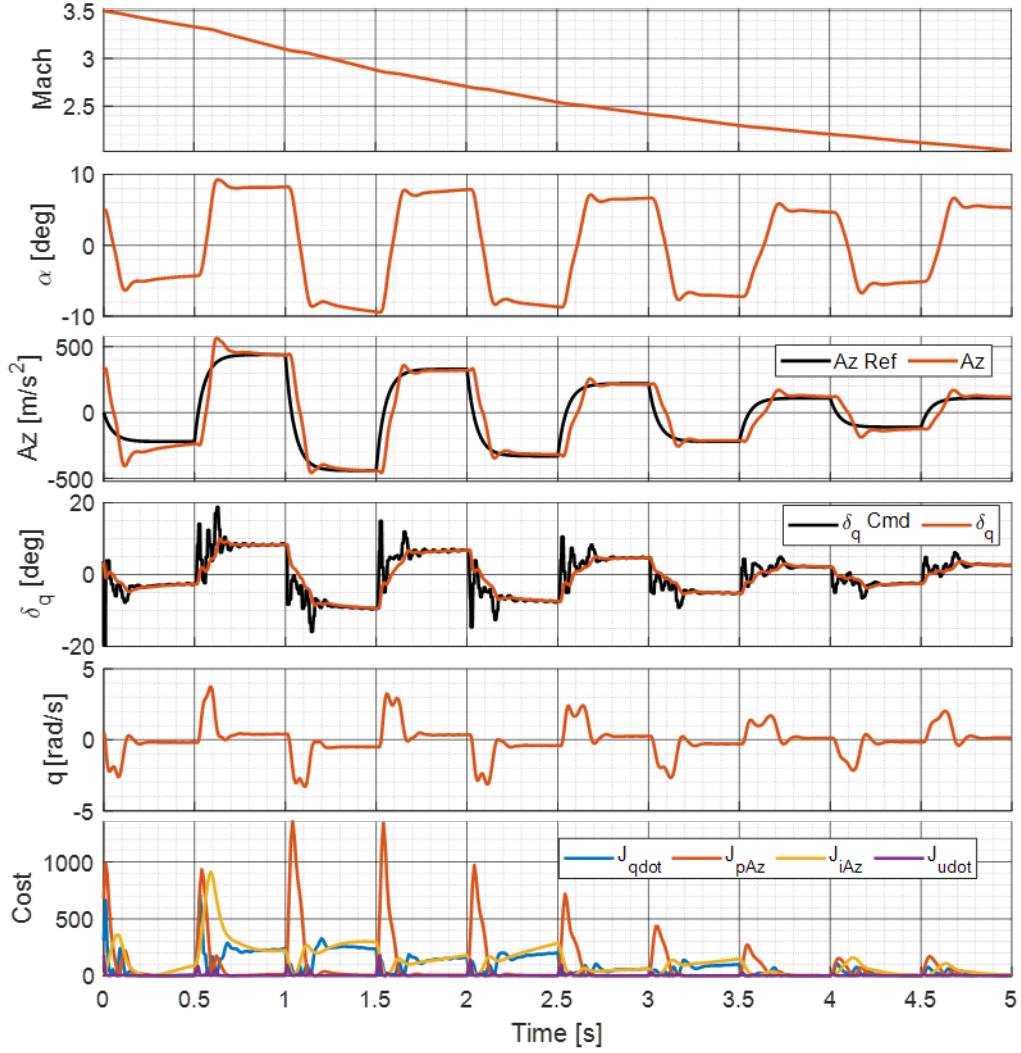


Fig. 4 Simulation results showing controller performance for \tilde{A}_z reference tracking for a simulated flight across the desired M, α flight envelope

7. Conclusion

In this report, an approach is presented to apply MPC to provide stabilization and command tracking for a high-speed projectile with nonlinear dynamics. An LPV model is identified to approximate the projectile dynamics for the online control optimization. The implementation of the MPC methodology is shown to yield promising performance across a M, α flight envelope using an LPV model derived from the nonlinear longitudinal dynamics.

Future research will extend this architecture to the full 6DoF system dynamics and explore the performance degradation due to sensor noise and model inaccuracies. Additionally, the flight envelope will be expanded to include the subsonic flight regime and a range of altitudes.

8. References

1. Costello M. Extended range of a gun launched smart projectile using controllable canards. *Shock Vibration*. 2001;8:203–213.
2. Fresconi FE. Range extension of gun-launched smart munitions. *International Ballistics Symposium*; 2008.
3. Bryson JT, Vasile JD, Celmins I, Fresconi FE. Approach for understanding range extension of gliding indirect fire munitions. *Atmospheric Flight Mechanics Conference*; 2018. AIAA Scitech Paper No.: 2018-3158.
4. Vasile JD, Bryson JT, Fresconi FE. Aerodynamic design optimization of long range projectile using missile DATCOM. *AIAA Scitech Forum*; 2021. AIAA Scitech Paper No.: 2020-1762.
5. Vasile J, Sahu J. Roll orientation-dependent aerodynamics of a long-range projectile. *DEVCOM Army Research Laboratory*; 2020 Aug. Report No.: ARL-TR-9017.
6. Vasile J, Bryson J, Sahu J, Paul J, Gruenwald B. Aerodynamic dataset generation of a long-range projectile. *DEVCOM Army Research Laboratory*; 2020 Aug. Report No.: ARL-TR-9019.
7. Zhou K, Doyle JC, Glover K. *Robust and optimal control*. Prentice Hall; 1996.
8. Morato MM, Normey-Rico JE, Sename O. Model predictive control design for linear parameter varying systems: a survey. *Ann Rev Control*. 2020;49:64–80.
9. Fresconi F, Ilg M. Model predictive control of agile projectiles. *AIAA Atmospheric Flight Mechanics Conference*; 2012. AIAA Paper No.: 2012-4860.
10. Xu Z, Zhao J, Qian J, Zhu Y. Nonlinear MPC using an identified LPV model. *Indust Eng Chem Res*. 2009;48(6):3043–3051.
11. Wada N, Saito K, Saeki M. Model predictive control for linear parameter varying systems using parameter dependent Lyapunov function. *IEEE Trans Circuits Sys II Express Briefs*. 2006 Dec;53(12):1446–1450. doi: 10.1109/TCSII.2006.883832.
12. Nelson RC. *Flight stability and automatic control*. 2nd Ed. McGraw-Hill; 1998.
13. Bossert DE, Morris SL, Hallgren WF, Yechout TR. *Introduction to aircraft flight mechanics*. AIAA; 2003.

14. Fresconi FE, Celmins I, Sifton SI. Theory, guidance, and flight control for high maneuverability projectiles. Army Research Laboratory (US); 2014 Jan. Report No.: ARL-TR-6767.
15. Tóth R. Modeling and identification of linear parameter-varying systems. Springer; 2010. Lecture Notes in Control and Information Sciences; vol. 403.
16. Rajan S, Wang S, Inkol R, Joyal A. Efficient approximations for the arctangent function. IEEE Signal Processing Magazine. 2006;23(3):108–111.
17. Andersson JA, Gillis J, Horn G, Rawlings JB, Diehl M. CasADi: a software framework for nonlinear optimization and optimal control. Math Prog Comput. 2019;11(1):1–36.
18. Wächter A, Biegler LT. On the implementation of an interior-point filter line-search algorithm for large-scale nonlinear programming. Math Prog. 2006;106(1):25–57.

Nomenclature

| | | |
|---------------|---|---|
| α | = | body angle of attack in pitch plane |
| \tilde{A}_z | = | specific aerodynamic force in z direction |
| C_D | = | coefficient for drag force |
| C_L | = | coefficient for lift force |
| C_m | = | coefficient of pitching moment |
| D | = | reference diameter |
| δ_q | = | pitch control deflection angle |
| I_y | = | transverse moment of inertia |
| M | = | Mach number |
| m | = | mass |
| q | = | pitch rate |
| Q | = | $\frac{1}{2} \rho V^2$, dynamic pressure |
| S | = | $D^2\pi/4$, aerodynamic reference area |
| θ | = | pitch angle |
| u | = | body velocity component in x direction |
| u_c | = | control input to state space model |
| w | = | body velocity component in z direction |
| X | = | force in the x direction (body frame) |
| Z | = | force in the z direction (body frame) |

List of Symbols, Abbreviations, and Acronyms

| | |
|------|-------------------------------|
| 6DoF | 6 degrees of freedom |
| AoA | angle of attack |
| CG | center of gravity |
| LPV | Linear Parameter Varying |
| LTV | Laboratory Technology Vehicle |
| MPC | Model Predictive Control |

1 DEFENSE TECHNICAL
(PDF) INFORMATION CTR
DTIC OCA

1 DEVCOM ARL
(PDF) FCDD RLD DCI
TECH LIB

18 DEVCOM ARL
(PDF) FCDD RLW A
F E FRESCONI
FCDD RLW W
T SHEPPARD
FCDD RLW WD
J T BRYSON
B C GRUENWALD
L STROHM
B BURCHETT
I CELMINS
J DESPIRITO
L FAIRFAX
J PAUL
J D VASILE
FCDD RLW WA
N TRIVEDI
FCDD RLW WB
J SADLER
FCDD RLW WC
M MINNICINO
FCDD RLW WE
M ILG
B TOPPER
D EVERSON
FCDD RLW WF
E RIGAS